the FEBS Journal

Bivalent binding drives the formation of the Grb2–Gab1 signaling complex in a noncooperative manner

Caleb B. McDonald, Vikas Bhat, David C. Mikles, Brian J. Deegan, Kenneth L. Seldeen and Amjad Farooq

Department of Biochemistry & Molecular Biology and the USylvester Braman Family Breast Cancer Institute, Leonard Miller School of Medicine, University of Miami, FL, USA

Keywords
intrinsic disorder; macromolecular assembly; multivalent binding; SH3–ligand interactions; zero cooperativity

Correspondence
A. Farooq, Department of Biochemistry & Molecular Biology and the USylvester Braman Family Breast Cancer Institute, Leonard Miller School of Medicine, University of Miami, Miami, FL 33136, USA
Fax: +1 305 2433955
Tel: +1 305 243 2429
E-mail: amjad@farooqlab.net

(Received 24 November 2011, revised 20 February 2012, accepted 11 April 2012)

doi:10.1111/j.1742-4658.2012.08600.x

Although the growth factor receptor binder 2 (Grb2)–Grb2-associated binder (Gab)1 macromolecular complex mediates a multitude of cellular signaling cascades, the molecular basis of its assembly has hitherto remained largely elusive. Herein, using an array of biophysical techniques, we show that, whereas Grb2 exists in a monomer–dimer equilibrium, the proline-rich (PR) domain of Gab1 is a monomer in solution. Of particular interest is the observation that although the PR domain appears to be structurally disordered, it nonetheless adopts a more or less compact conformation reminiscent of natively folded globular proteins. Importantly, the structurally flexible conformation of the PR domain appears to facilitate the binding of Gab1 to Grb2 with a 1 : 2 stoichiometry. More specifically, the formation of the Grb2–Gab1 signaling complex is driven via a bivalent interaction through the binding of the C-terminal homology 3 (cSH3) domain within each monomer of Grb2 homodimer to two distinct RXXK motifs, herein designated G1 and G2, located within the PR domain of Gab1. Strikingly, in spite of the key role of bivalency in driving this macromolecular assembly, the cSH3 domains bind to the G1 and G2 motifs in an independent manner with zero cooperativity. Taken together, our findings shed new light on the physicochemical forces driving the assembly of a key macromolecular signaling complex that is relevant to cellular health and disease.

Structured digital abstract

- GRB2 and GRB2 bind by light scattering (View interaction)
- GAB1 and GRB2 bind by isothermal titration calorimetry (View Interaction: 1, 2, 3)

Introduction

The growth factor receptor binder 2 (Grb2)–Grb2-associated binder (Gab)1 interaction mediates signaling between upstream cell surface receptor tyrosine kinases (RTKs) and downstream effectors such as Ras and Akt that are involved in a diverse array of cellular activities, including growth, survival, proliferation, and oncogenic transformation [1–6]. Indeed, the disruption of the *grb2* and *gab1* genes results in numerous developmental defects in mice, and their overexpression is implicated in the genesis of human breast cancer

Abbreviations

ALS, analytical light scattering; cSH3, C-terminal homology 3; DLS, dynamic light scattering; Gab, growth factor receptor binder 2-associated binder; Grb2, growth factor receptor binder 2; ITC, isothermal titration calorimetry; MAPK, mitogen-activated protein kinase; MD, molecular dynamics; M_n, number-average molar mass; M_w, weighted-average molar mass; nSH3, N-terminal Src homology 3; PDB, Protein Data Bank; PH, pleckstrin homology; PPII, polyproline type II; PR, proline-rich; rmsf, root mean square fluctuation; RTK, receptor tyrosine kinase; SH2, Src homology 2; SH3, Src homology 3; SLS, static light scattering; Sos1, Son of sevenless 1.

[7–12]. Importantly, proteins involved in mediating cellular signaling usually have a modular architecture, and this also holds true for Grb2 and Gab1. Thus, Grb2 is constructed on the N-terminal Src homology 3 (nSH3)–Src homology 2 (SH2)–C-terminal Src homology 3 (cSH3) signaling module, and Gab1 is composed of the pleckstrin homology (PH)–proline-rich (PR) signaling cassette.

The modular structure of Grb2 and Gab1 is exquisitely suited for their participation in a diverse array of signaling cascades that are central to health and disease. In particular, Grb2 adaptor recognizes activated cell surface RTKs such as hepatocyte growth factor receptor, epidermal growth factor receptor, fibroblast growth factor receptor and platelet-derived growth factor receptor by virtue of its SH2 domain's ability to bind to tyrosine-phosphorylated (pY) sequences in the context of pYXN motifs located within the receptor tails on the cytoplasmic face of the membrane [13,14]. Upon binding to RTKs, the Src homology 3 (SH3) domains of Grb2 recruit a wide variety of proteins containing PR sequences to the inner membrane surface – the site of initiation of a multitude of signaling cascades [15–23]. Among them, the son of sevenless 1 (Sos1) guanine nucleotide exchange factor and the Gab1 docking protein are by far the best characterized downstream partners of Grb2 [15–18]. Upon recruitment to the inner membrane surface, Sos1 facilitates the GDP–GTP exchange within the membrane-bound Ras GTPase, and thereby switches on a key signaling circuit that involves the activation of the mitogen-activated protein kinase (MAPK) cascade, which is central to cellular growth and proliferation [24]. In contrast, the recruitment of Gab1 to the inner membrane surface provides docking platforms for the Shp2 tyrosine phosphatase and phosphoinositide 3-kinase, which respectively account for further amplification of Ras activity, as sustained activation of Ras requires both the Sos1-dependent and Gab1-dependent pathways [1,25,26], and the activation of Akt serine-threonine kinase, which plays an important role in cell growth and survival [27]. Although the Grb2–Gab1 interaction is believed to occur through the binding of the cSH3 domain of Grb2 to an atypical RXXK motif within the PR domain of Gab1 [18,28], the precise mechanism underlying the assembly of this key signaling complex has hitherto remained poorly understood. Of particular note is the demonstration that the cSH3 domain of Grb2 recognizes two distinct RXXK motifs, herein designated G1 and G2 (Fig. 1), within the PR domain of Gab1 in a physiologically relevant manner [29]. This salient observation, coupled with the knowledge that Grb2 exists in a dimer–monomer equilibrium in solution [30], raises the possibility that the assembly of the Grb2–Gab1 signaling complex may be driven through multivalent binding leading to the formation of higher-order Grb2–Gab1 multimers rather than a simple binary complex.

The present study was undertaken in an attempt to further our understanding of the assembly of the Grb2–Gab1 signaling complex. Herein, using an array of biophysical techniques, we show that, whereas Grb2 exists in a monomer–dimer equilibrium, the PR domain of Gab1 is a monomer in solution. Of particular interest is the observation that although the PR domain appears to be structurally disordered, it nonetheless adopts a more or less compact conformation reminiscent of natively folded globular proteins. Importantly, the structurally flexible conformation of the PR domain appears to facilitate the binding of Gab1 to Grb2 with a 1 : 2 stoichiometry. More specifically, the formation of the Grb2–Gab1 signaling complex is driven via a bivalent interaction through the binding of the cSH3 domain within each monomer of the Grb2 homodimer to two distinct RXXK motifs, herein designated G1 and G2, located within the PR domain of Gab1. Strikingly, in spite of the key role of bivalency in driving this macromolecular assembly, the cSH3 domains bind to the G1 and G2 motifs in an independent manner, with zero cooperativity. Taken together, our findings shed new light on the physicochemical forces driving the assembly of a key macromolecular signaling complex that is relevant to cellular health and disease.

Results and Discussion

The PR domain of Gab1 is a monomer in solution

In order to understand the assembly of the Grb2–Gab1 complex, we first conducted analytical light scattering (ALS) analysis on wild-type full-length Grb2 (Grb2_WT) and the wild-type PR domain of Gab1 (PR_WT), so as to assess their propensities to associate into higher-order oligomers in solution (Fig. 2). Our data suggest that, whereas Grb2 exists in a monomer–dimer equilibrium, in agreement with our previous study [30], the PR domain of Gab1 is a monomer in solution (Tables 1 and 2). In an attempt to gain insights into the macromolecular polydispersity and shape of the various species, we also determined the corresponding weighted-average molar mass (M_w)/number-average molar mass (M_n) ratios and hydrodynamic radii from our data. Our analysis revealed that both the monomeric and dimeric forms of Grb2, as well as the PR domain, display M_w/M_n

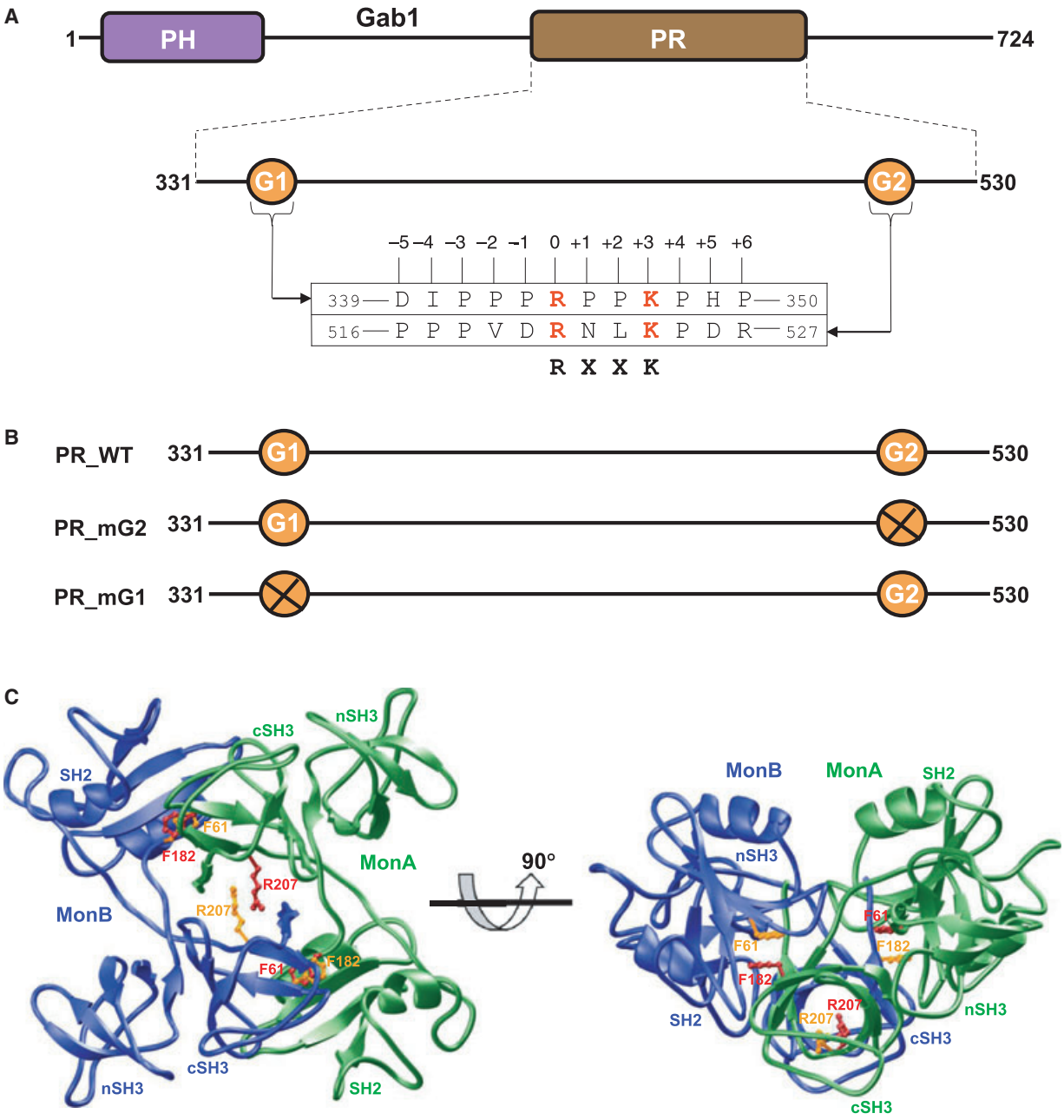

Fig. 1. An overview of the various constructs of full-length Grb2 and the PR domain of Gab1 used in this study. (A) Gab1 contains an N-terminal PH domain and a C-terminal PR domain flanked by long stretches of uncharacterized regions. The PR domain contains two distinct RXXK motifs, herein designated G1 and G2. The amino acid sequences of these motifs and flanking residues within Gab1 are provided. The numbering of various residues within and flanking the RXXK motifs is based on the nomenclature suggested by Feller *et al.* [47]. (B) Maps of the various constructs of the PR domain of Gab1. In addition to the wild-type PR domain construct (PR_WT), which contains both native G1 and G2 motifs, constructs were designed in which the G2 (PR_mG2) and G1 (PR_mG1) motifs were individually mutated, through alanine substitution of arginines and lysines within the corresponding RXXK consensus sequence, so as to abrogate their binding to the cSH3 domain of Grb2. Note that the numerals at the ends of each construct indicate amino acid sequence numbers within human Gab1. (C) 3D structure of the Grb2 homodimer with a two-fold axis of symmetry as solved by Ducruix *et al.* [31]. One monomer of Grb2 is shown in green (MonA) and the other in blue (MonB). The various domains within the nSH3–SH2–cSH3 modular cassette of each Grb2 monomer are labeled for clarity. The side chain moieties of Phe61/Phe182/Arg207, the three most likely candidates involved in buttressing intermolecular contacts at the monomer–monomer interface and subjected to alanine substitution, are colored red (MonA) and yellow (MonB).

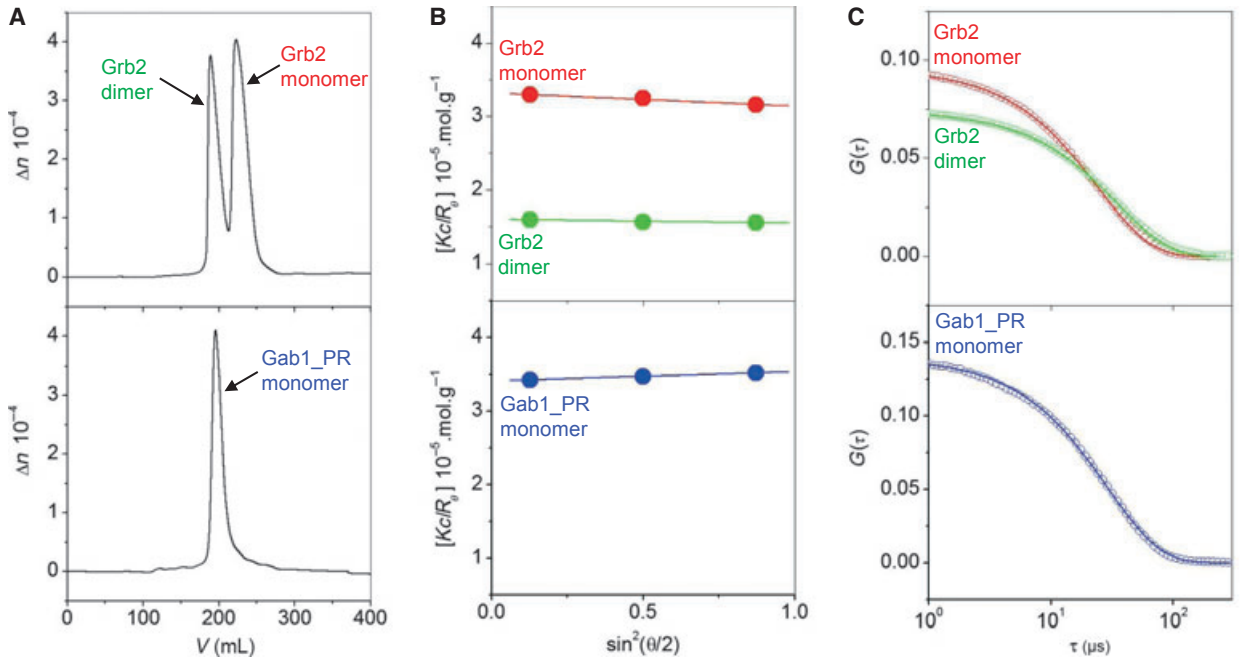

Fig. 2. ALS analysis of full-length Grb2 and the PR domain of Gab1 (Gab1_PR). (A) Elution profiles as monitored by the differential refractive index (Δn) plotted as a function of elution volume (V) for Grb2 (top panel) and Gab1_PR (bottom panel). Note that Grb2 elutes as two distinct species corresponding to a dimer and a monomer, whereas Gab1_PR domain elutes as a single monomeric species. (B) Partial Zimm plots obtained from analytical SLS measurements at a specific protein concentration for the Grb2 dimer and monomer (top panel) and the Gab1_PR monomer (bottom panel). The solid lines through the data points represent linear fits. (C) Autocorrelation function plots obtained from analytical DLS measurements at a specific protein concentration for the Grb2 dimer and monomer (top panel) and the Gab1_PR monomer (bottom panel). The solid lines through the data points represent nonlinear least squares fits to Eqn (6).

Table 1. Hydrodynamic parameters obtained from ALS measurements for wild-type and various mutant constructs of full-length Grb2. Note that the molecular mass of recombinant full-length Grb2 calculated from the amino acid sequence alone is 30 kDa. Errors were calculated from at least three independent measurements. All errors are given to one standard deviation.

	Associativity	M_w (D)	M_n (D)	M_w/M_n	D_t ($\mu m^2 \cdot s^{-1}$)	R_h (Å)
Grb2_WT	Monomer	31 000 ± 1000	30 000 ± 1000	1.02 ± 0.03	64 ± 1	38 ± 1
	Dimer	63 000 ± 2000	61 000 ± 2000	1.02 ± 0.01	46 ± 1	53 ± 1
Grb2_F61A	Monomer	34 000 ± 2000	33 000 ± 1000	1.01 ± 0.01	58 ± 1	41 ± 1
	Dimer	58 000 ± 1000	57 000 ± 1000	1.02 ± 0.01	45 ± 1	53 ± 1
Grb2_F182A	Monomer	31 000 ± 1000	31 000 ± 1000	1.00 ± 0.01	62 ± 1	39 ± 1
	Dimer	54 000 ± 1000	54 000 ± 1000	1.00 ± 0.01	43 ± 1	56 ± 1
Grb2_R207A	Monomer	30 000 ± 1000	30 000 ± 1000	1.00 ± 0.02	62 ± 1	39 ± 1
	Dimer	56 000 ± 1000	55 000 ± 1000	1.02 ± 0.01	42 ± 1	57 ± 1

Table 2. Hydrodynamic parameters obtained from ALS measurements for wild-type and various mutant constructs of the PR domain of Gab1. Note that the molecular mass of the recombinant PR domain of Gab1 calculated from the amino acid sequence alone is 27 kDa. Errors were calculated from at least three independent measurements. All errors are given to one standard deviation.

	Associativity	M_w	M_n	M_w/M_n	D_t ($\mu m^2 \cdot s^{-1}$)	R_h (Å)
PR_WT	Monomer	28 000 ± 1000	27 000 ± 2000	1.04 ± 0.02	53 ± 1	47 ± 1
PR_mG2	Monomer	26 000 ± 2000	26 000 ± 3000	1.01 ± 0.01	55 ± 1	44 ± 1
PR_mG1	Monomer	29 000 ± 1000	28 000 ± 1000	1.03 ± 0.01	53 ± 1	47 ± 1

ratios close to unity, implying that they are all highly monodisperse in solution. Furthermore, the hydrodynamic radii observed for the Grb2 monomer and dimer are consistent with their tightly packed αβ-folds [31].

Remarkably, the hydrodynamic radius observed for the PR domain of Gab1 lies somewhere between those of monomeric and dimeric Grb2 (Table 2), implying that the PR domain adopts a compact shape in a manner akin to that adopted by globular proteins, rather than an extended random coil-like conformation devoid of any structural features. This observation is particularly surprising in that the PR proteins, such as the PR domain of Gab1, are believed to be devoid of any intrinsic structure in solution. This is attributable to the rigidity of the proline side chain, which is structurally destabilizing but nevertheless allows PR proteins to adopt a rigid conformation that is ideally suited for binding to cognate ligands at the expense of little entropic penalty, which is often the bottleneck in protein–protein interactions that are relevant to cellular signaling cascades. The fact that the PR domain of Gab1 appears to be compact and globular in solution suggests strongly that the lack of secondary structural elements such as α-helices and β-strands may not necessarily equate to lack of intrinsic structure. On the contrary, our data support the notion that PR proteins may be able to adopt a compact shape, and that such adoption may be a necessity to avoid chaos within the cellular environment, where the high concentration of PR sequences and proteins in general may otherwise increase cellular entropy through intrinsic disorder and the formation of structural knots.

In order to evaluate the extent to which the integrity of the G1 and G2 motifs is required for the PR domain of Gab1 to adopt a compact globular-like conformation, we also conducted ALS analysis on PR_mG2 and PR_mG1 mutant constructs of the PR domain, and compared various hydrodynamic parameters with those obtained for PR_WT (Fig. 1B). Our data show that mutation of the G1 and G2 motifs has no apparent effect on the hydrodynamic radius of the PR domain (Table 2), implying that these motifs do not play a direct role in the ability of the PR domain to attain a compact fold. Next, we also made an attempt to disrupt the monomer–monomer interface within the Grb2 homodimer, so as to generate a mutant protein that is largely monomeric in solution for subsequent analysis. The 3D structure of the Grb2 homodimer, as solved by Ducruix *et al.* [31] (Fig. 1C), suggests that the Phe61/Phe182/Arg207 triad within each monomer may play a key role in reinforcing and buttressing the monomer–monomer contacts. Thus, not only does the phenyl moiety of Phe61 within one monomer stack against the phenyl moiety of Phe182 within the other monomer via van der Waals contacts at the monomer–monomer interface, but the aliphatic side chains of Arg207 within each monomer also experience a similar fate. In light of this, we generated Grb2_F61A, Grb2_F182A and Grb2_R207A single-alanine mutant constructs, and analyzed and compared their hydrodynamic properties with those of the Grb2_WT construct (Table 1). To our surprise, all three mutant constructs of Grb2 failed to shift the dimer–monomer equilibrium in favor of the latter. Further work is clearly warranted to unearth the molecular basis of Grb2 dimerization, as this not only has direct relevance to understanding how Grb2 binds its ligands, but could also potentially lead to the development of a protein with therapeutic potential.

Intrinsic disorder reigns within the PR domain of Gab1

The PR domain of Gab1 is abundant in residues such as proline and polar and charged residues, which are usually found in structurally disordered proteins. Given its key role in the Ras–MAPK pathway, it is fitting that the PR domain of Gab1 shares this characteristic with other structurally disordered proteins that are believed to play a central role in mediating cellular signaling cascades [32–36]. In an attempt to further analyze the extent of structural disorder within the PR domain of Gab1, we performed secondary structure prediction analysis using POODLE [37]. As shown in Fig. 3A, our analysis revealed that the PR domain is indeed predominantly disordered, and lacks any identifiable α-helical and/or β-strand features that are characteristic of well-folded αβ-proteins. This salient observation is further corroborated by our far-UV CD analysis (Fig. 3B), wherein the spectrum of the PR domain shows a minimum centered around 208 nm, a signature that is usually characteristic of proteins containing random coil and polyproline type II (PPII) helical conformations [38,39]. Additionally, the rather broad far-UV CD spectrum of the PR domain suggests that it is conformationally heterogeneous, as would be expected for structurally disordered proteins without a well-defined compact fold.

Grb2 binds to the PR domain of Gab1 with a 2 : 1 stoichiometry

The Grb2–Gab1 interaction is believed to occur through the binding of the cSH3 domain of Grb2 to an atypical RXXK motif within the PR domain of

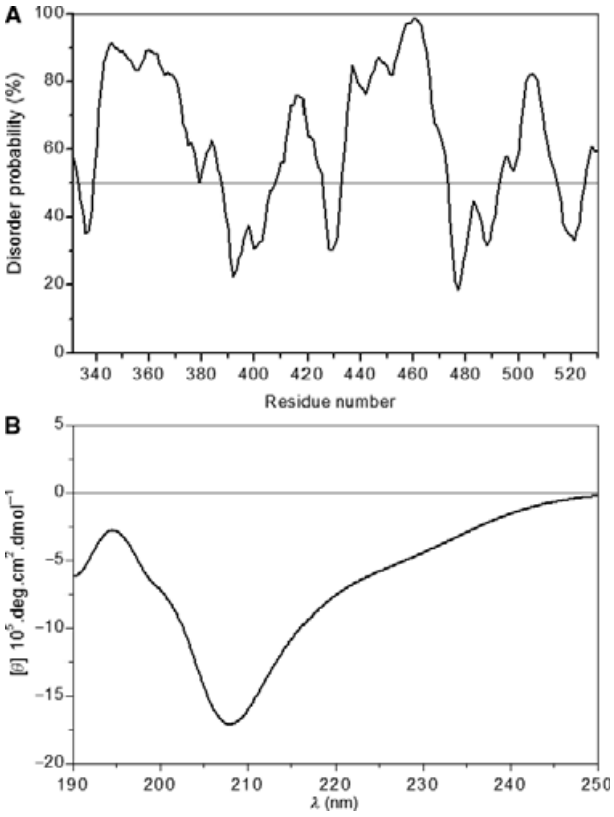

Fig. 3. Secondary structure analysis of the PR domain of Gab1. (A) *In silico* prediction of intrinsic disorder within the PR domain. (B) Experimentally determined far-UV CD spectrum of the PR domain.

Gab1 [18,28]. Importantly, we previously demonstrated that the cSH3 domain of Grb2 recognizes two distinct RXXK motifs, herein designated G1 and G2 (Fig. 1A), within the PR domain of Gab1 in a physiologically relevant manner [29]. To understand the stoichiometry and underlying thermodynamic forces driving the binding of Grb2 to Gab1, we next measured the binding of full-length Grb2 to the PR domain of Gab1, using isothermal titration calorimetry (ITC) (Fig. 4). Our analysis revealed that Grb2 binds to PR_WT, containing both G1 and G2 sites, with a 2 : 1 stoichiometry (Table 3). Coupled with previous data [18,28,29], the most straightforward interpretation of this finding is that Grb2 binds in a bivalent manner to Gab1 to form the Grb2–Gab1 complex with a 2 : 1 stoichiometry, and that this interaction is mediated through the binding of the cSH3 domain within each Grb2 molecule to each of the two distinct RXXK motifs (G1 and G2) within Gab1. Given that the PR domain of Gab1 adopts a compact shape, and that Grb2 displays the propensity to homodimerize in solution (Fig. 2), the 2 : 1 stoichiometry observed here may not necessarily be attributable to the binding of the cSH3 domain within each molecule of Grb2 to both G1 and G2 sites. On the contrary, it is highly plausible that the binding of the PR domain through one of its two RXXK motifs to the cSH3 domain of one monomer within the Grb2 homodimer sterically blocks the binding of the second monomer to another PR domain, so as to prevent the formation of the Grb2–Gab1 complex with a 2 : 2 stoichiometry.

To test the extent to which the formation of the Grb2–Gab1 complex with a 2 : 1 stoichiometry may be influenced by steric hindrance, we also measured the binding of full-length Grb2 to mutant PR constructs, in which either the G1 site (PR_mG1) or the G2 site (PR_mG2) has been mutated (Table 3). Our data show that Grb2 binds to both PR_mG1 and PR_mG2 constructs with a 1 : 1 stoichiometry, implying that the formation of the Grb2–Gab1 complex with a 2 : 1 stoichiometry is indeed driven through the binding of both G1 and G2 motifs within the PR domain to the cSH3 domain within each molecule of Grb2. Furthermore, our data also suggest that the formation of the Grb2–Gab1 complex is driven by favorable enthalpic changes accompanied by entropic penalty. This implies that specific intermolecular hydrogen bonding and ion pairing interactions predominate over hydrophobic forces in mediating the association of Grb2 with Gab1, in agreement with our previous report [29].

Bivalent binding of Grb2 to the PR domain of Gab1 is not governed by cooperativity

Our ITC data suggested that Grb2 binds to the G2 motif with an affinity that is nearly an order of magnitude greater than that observed for binding to the G1 motif (Table 3), implying that the PR domain of Gab1 contains a high-affinity G2 site and a low-affinity G1 site for latching onto Grb2. Given that the formation of the Grb2–Gab1 complex occurs through bivalent binding, it is tempting to invoke the role of cooperativity in driving the assembly of this key signaling complex. Thus, for cooperative binding, the affinity of binding of Grb2 to PR_WT, containing both the G1 and G2 sites, should be expected to be much higher than that observed for binding to each individual site, owing to entropic advantage. To our surprise, our data indicated that binding of Grb2 to PR_WT occurs with an affinity that is greater than that observed for its binding to the G1 site, but lower that observed for its binding to the G2 site, or essentially an average of the two constituent affinity terms (Table 3). In order to understand the role of cooperativity in driving the formation of the Grb2–Gab1 complex in more

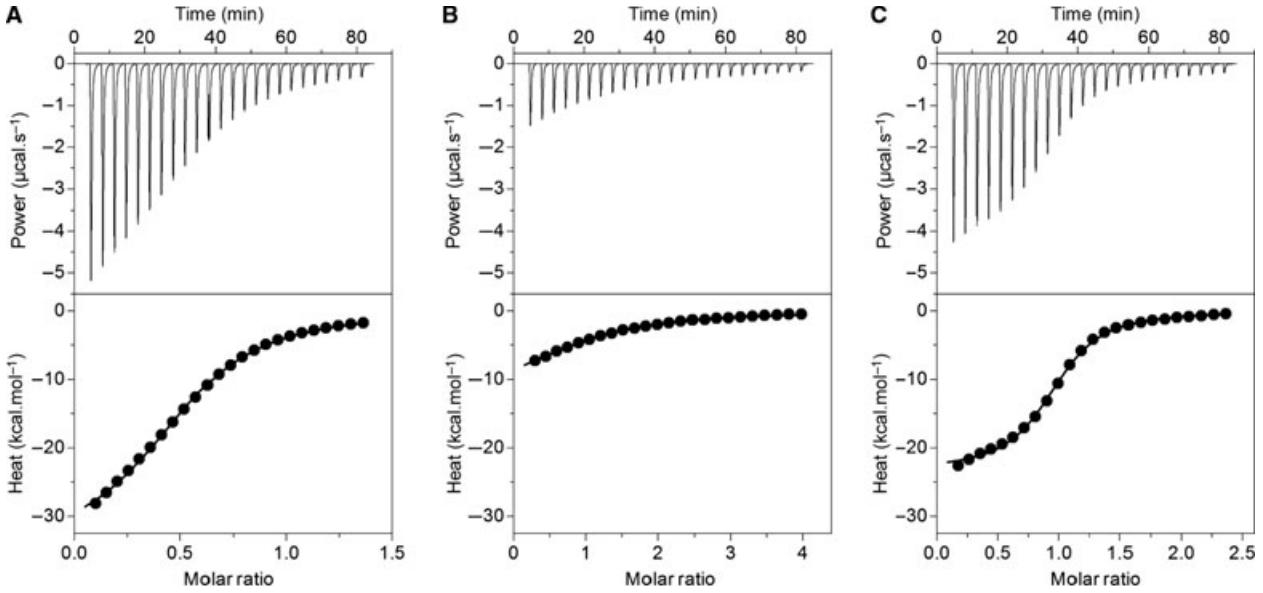

Fig. 4. ITC analysis of the binding of full-length Grb2 to PR_WT (A), PR_mG2 (B) and PR_mG1 (C) constructs of Gab1. The upper panels show raw ITC data expressed as change in thermal power with respect to time over the period of titration. In the lower panels, the change in molar heat is expressed as a function of the molar ratio of the corresponding PR construct to Grb2. The solid lines in the lower panels show the fit of data to a one-site model, as embodied in Eqn (11), with ORIGIN.

Table 3. Thermodynamic parameters obtained from ITC measurements for the binding of wild-type and mutant constructs of the PR domain of Gab1 to full-length Grb2. Note that *n* is the stoichiometry of full-length Grb2 bound to each PR construct. Errors were calculated from at least three independent measurements. All errors are given to one standard deviation. NA, not applicable.

	n	K_d (μM)	ΔH (kcal·mol^{-1})	$T\Delta S$ (kcal·mol^{-1})	ΔG (kcal·mol^{-1})	$\Delta\Delta G_c$ (kcal·mol^{-1})
PR_WT	1.94 ± 0.05	7.21 ± 0.44	−34.47 ± 0.09	−20.42 ± 0.16	−14.04 ± 0.07	+0.09 ± 0.08
PR_mG2	1.02 ± 0.04	20.26 ± 1.70	−13.21 ± 0.12	−6.80 ± 0.07	−6.41 ± 0.05	NA
PR_mG1	1.07 ± 0.03	2.24 ± 0.23	−23.37 ± 0.24	−15.65 ± 0.18	−7.72 ± 0.06	NA

quantitative terms, we also calculated the contribution of cooperative interactions to the overall free energy of binding. Consistent with the foregoing argument, the free energy of cooperativity ($\Delta\Delta G_c$) associated with the formation of the Grb2–Gab1 complex is close to zero (Table 3), implying that the cSH3 domains within two individual Grb2 molecules bind to two RXXK motifs within Gab1 in an independent manner. That this is so is further corroborated by the fact that the underlying enthalpic (ΔH) and entropic ($T\Delta S$) contributions to the overall free energy (ΔG) of binding of Grb2 to PR_WT more or less equal the sum of the corresponding thermodynamic terms associated with the binding of Grb2 to the G1 and G2 sites in the context of mutant PR domains.

We also note that although binding of RXXK motifs within the PR domain of Gab1 to Grb2 appears to occur in an independent manner with zero cooperativity, it is nonetheless context-dependent. Thus, in conjunction with our previous study [29], it seems that RXXK motifs in the context of the PR domain bind to cSH3 domains of Grb2 with affinities that are an order of magnitude greater than those observed for their binding in the context of isolated peptides. That this is so strongly argues that regions outside the canonical RXXK motifs play an integral role in mediating the Grb2–Gab1 interaction in addition to site-specific interactions. It may well also be the case that the RXXK motifs depart from their physiological behavior when treated as short peptides, owing to the loss of the local conformational constraints that they may be subject to in the context of the PR domain or full-length Gab1. This notion is further supported by the observation that the PR domain adopts a compact shape, and is therefore likely to impart entropic advantage by virtue of its ability to restrict the degrees of freedom available

to RXXK motifs. Importantly, such a synergistic effect has also been observed upon the binding of a PR sequence within phosphoinositide 3-kinase to the SH3 domain of Fyn kinase [40]. In short, our data suggest that the bivalent binding of cSH3 domains of two individual Grb2 molecules to two distinct RXXK motifs within Gab1 occurs in an independent manner without any cooperative interactions.

Structural basis of the binding of Grb2 to the PR domain of Gab1 as two independent monomers versus a homodimer

Our thermodynamic data suggest that the bivalent binding of Grb2 to Gab1 with a 2 : 1 stoichiometry is not under cooperative control, but is rather driven through the binding of cSH3 domains within two individual molecules of Grb2 to two distinct RXXK motifs within the PR domain of Gab1 in an independent manner. On the other hand, our hydrodynamic data indicate that Grb2 exists in a monomer–dimer equilibrium in solution. In light of these observations, it is thus conceivable that Grb2 could bind to the PR domain of Gab1 either as two independent monomers (Grb2–PR–Grb2) or as a homodimer [$(Grb2)_2$–PR]. To gain insights into the structural basis of the binding of Grb2 to the PR domain as two independent monomers, and to compare this mode of binding to that of a homodimer, we built appropriate structural models of Grb2 in complex with the PR domain of Gab1 (Fig. 5). Our structural models suggest that the canonical hydrophobic grooves within the cSH3 domains of Grb2 that accommodate the RXXK ligands are fully exposed to solution in the context of both the monomers and homodimer, implying that it is indeed physically feasible for Grb2 to bind to the PR domain both as two independent monomers and as a homodimer. Importantly, the monomers within the Grb2 homodimer adopt a two-fold axis of symmetry, such that the SH2 domain of one monomer docks against the cSH3 domain of the other and vice versa in a head-to-tail fashion, as observed in the crystal structure determined by Ducruix *et al.* [31].

It should be noted that the G1 and G2 motifs within the PR domain of Gab1 bind to the cSH3 domain of Grb2 with distinct mechanisms, as reported previously [29]. Thus, whereas the G1 motif strictly requires the PPRPPKP consensus sequence for high-affinity binding to the cSH3 domain, the G2 motif displays a preference for the PXVXRXLKPXR consensus sequence. Although both the G1 and G2 motifs are accommodated within the same hydrophobic groove located within the β-barrel fold of each cSH3 domain, there are some notable differences in their modes of binding. Thus, whereas the G1 motif adopts the relatively open PPII-helical conformation upon binding to the cSH3 domain, the G2 motif assumes a much tighter 3_{10}-helical conformation (Fig. 5A,B). Remarkably, despite such distinguishing conformations, the nature of the residues within each cSH3 domain involved in interacting with the G1 and G2 motifs shows substantial similarities. Importantly, the Arg344/Arg521 and Lys347/Lys524 basic residues within the RXXK consensus sequence at the G1 and G2 sites are engaged, respectively, in close intermolecular hydrogen bonding and/or ion pairing contacts with Glu174 and Glu171 acidic residues located within the hydrophobic groove of each cSH3 domain. Additionally, aliphatic side chains of Arg344/Arg521 and Lys347/Lys524 within RXXK motifs also, respectively, associate with the benzyl ring of Phe167 and the indole moiety of Trp193 within each cSH3 domain through intermolecular van der Waals contacts. Finally, numerous residues within and flanking the RXXK motifs at both the G1 and G2 sites further engage in an intricate network of intermolecular contacts with their counterparts lining the hydrophobic groove within each SH3 domain in stabilizing these key SH3–ligand interactions, as fully discussed previously [29].

We note that although the spatial orientations of both RXXK motifs relative to the cSH3 domains within Grb2 monomers or homodimer can be relied upon with a high degree of confidence at the atomic level, because they were modeled on the basis of high sequence identity with corresponding templates, there is a high probability of uncertainty in the relative orientation and conformation of the intervening polypeptide chain spanning the G1 and G2 sites within the PR domain of Gab1. Notably, this intervening polypeptide chain was folded into a compact globular-like topology, in agreement with our hydrodynamic data, on the basis of *ab initio* modeling without any template. Despite such shortcomings, our structural models provide physical insights into the bivalent binding of the Grb2 adaptor to Gab1 docking protein, and provide a much anticipated structural framework for further understanding of the assembly of this key signaling complex.

Molecular dynamics (MD) simulations support the binding of Grb2 to the PR domain as a homodimer instead of two independent monomers

In an attempt to test the validity of our structural models and to shed light on the macromolecular dynamics underlying the assembly of the Grb2–Gab1

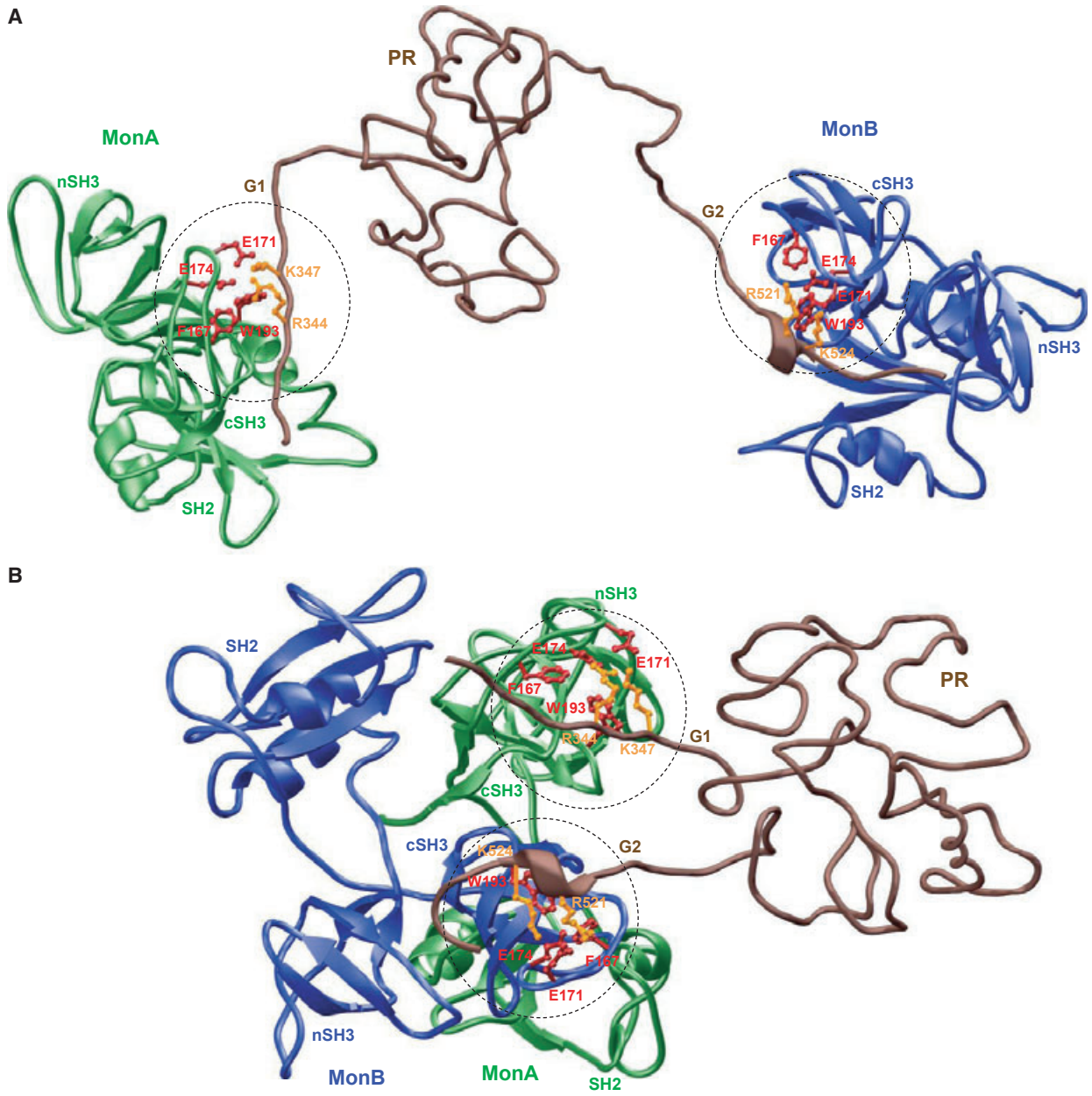

Fig. 5. Structural models of Grb2 bound to the G1 and G2 sites within the PR domain of Gab1, either as two isolated monomers (Grb2–PR–Grb2) (A), or in the context of a homodimer [$(Grb2)_2$–PR] (B). One monomer of Grb2 is shown in green (MonA) and the other in blue (MonB). The PR domain of Gab1 is colored brown. The interfaces between the hydrophobic grooves within the cSH3 domains of Grb2 monomers accommodating the RXXK motifs within the G1 and G2 sites are marked by dashed circles. Notably, the side chain moieties of arginines and lysines within the RXXK motifs at the G1 and G2 sites are colored yellow. The side chain moieties of residues within the cSH3 domains of Grb2 that interact with arginines and lysines within the RXXK motifs are colored red.

signaling complex, we performed MD simulations on structural models of Grb2 bound to the PR domain of Gab1, either as two independent monomers (Grb2–PR–Grb2) or as a homodimer [$(Grb2)_2$–PR] (CCFig. 6). Importantly, we assessed the stability and dynamics of various complexes and their constituent components in terms of both the rmsd of backbone atoms as a function of simulation time and root mean square fluctuation (rmsf) of backbone atoms as a function of residue number along each protein chain. As shown in Fig. 6A, the MD trajectories reveal that whereas the $(Grb2)_2$–PR complex asymptotically

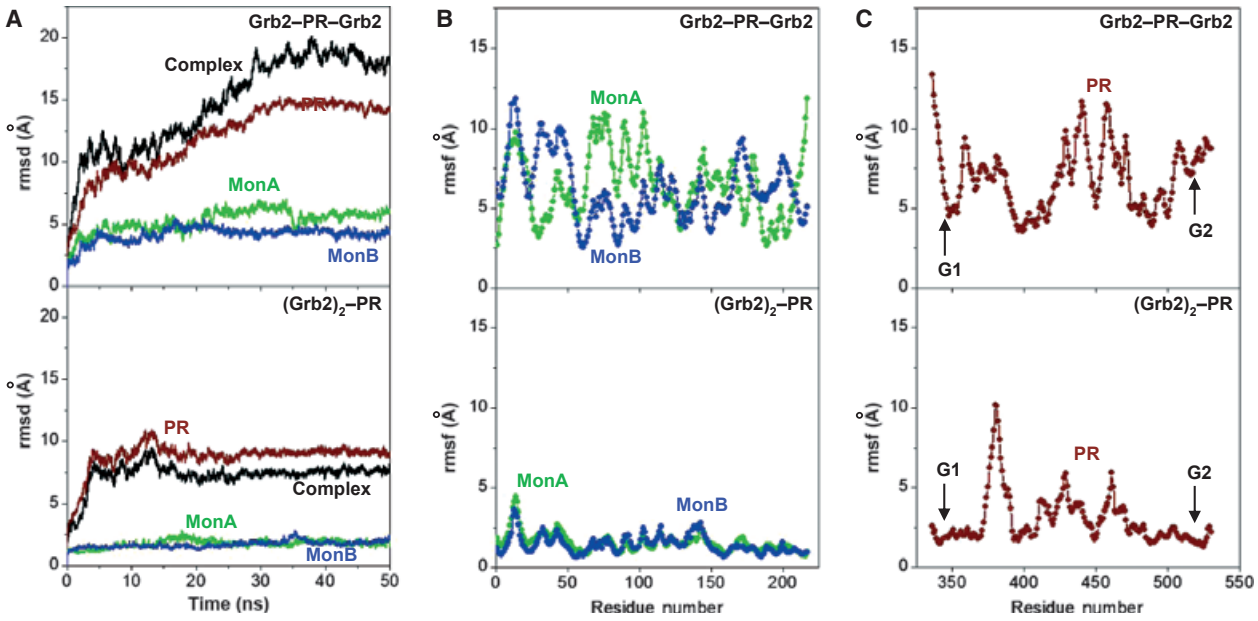

Fig. 6. MD analysis of Grb2 bound to the G1 and G2 sites within the PR domain of Gab1, either as two independent monomers (Grb2–PR–Grb2) or in the context of a homodimer [$(Grb2)_2$–PR]. (A) Rmsd values of backbone atoms (N, Cα, and C) within each simulated structure relative to the initial modeled structures of Grb2–PR–Grb2 (top panel) and $(Grb2)_2$–PR (bottom panel) complexes as a function of simulation time. Note that the overall rmsd for each complex (black) is deconvoluted into the PR domain (brown) and each of the two Grb2 monomers, designated MonA (green) and MonB (blue). (B) Rmsf of backbone atoms (N, Cα, and C) averaged over the entire course of corresponding MD trajectories of Grb2–PR–Grb2 (top panel) and $(Grb2)_2$–PR (bottom panel) complexes as a function of residue number within each of the two Grb2 monomers, designated MonA (green) and MonB (blue). (C) Rmsf of backbone atoms (N, Cα, and C) averaged over the entire course of corresponding MD trajectories of Grb2–PR–Grb2 (top panel) and $(Grb2)_2$–PR (bottom panel) complexes as a function of residue number within the PR domain (brown). Note that the vertical arrows indicate the location of the G1 and G2 motifs within the PR domain.

equilibrates with an rmsd of ~ 7 Å after ~ 20 ns, the Grb2–PR–Grb2 complex displays structural instability, with an rmsd of > 15 Å, even after 100 ns of simulation time. Simply put, these observations strongly argue that the Grb2 homodimer bound to the PR domain of Gab1 is structurally more stable than Grb2 monomers.

To understand the origin of such differential stabilities, we next deconvoluted the overall rmsd of each complex into its three constituent components: the PR domain of Gab1 and Grb2 monomers, designated MonA and MonB. Remarkably, our analysis revealed that the enhanced stability of the $(Grb2)_2$–PR complex arises from the enhanced stability of both the PR domain and monomers within the Grb2 dimer relative to their stabilities within the Grb2–PR–Grb2 complex. Thus, whereas Grb2 monomers in the context of a Grb2 homodimer bound to the PR domain display relatively high stability, with an rmsd of ~ 1.5 Å over the entire course of MD simulation, they appear to be highly unstable, with an rmsd of ~ 5 Å, when bound to the PR domain as two independent monomers. Likewise, the PR domain of Gab1 structurally stabilizes with an rmsd of ~ 8 Å, and remains relatively unstable, with an rmsd of ~ 15 Å, over the course of MD simulation. These observations were further corroborated through our rmsf analysis (Fig. 6B), wherein the distribution of atomic fluctuations within each residue of Grb2 monomers was monitored over the entire course of MD simulation. Thus, whereas a majority of residues within Grb2 monomers in the context of the $(Grb2)_2$–PR complex fluctuate with an rmsf of < 2 Å, this value rises to > 4 Å in the context of the Grb2–PR–Grb2 complex. Strikingly, our rmsf analysis also revealed that the residues within the PR domain of Gab1 in the context of the $(Grb2)_2$–PR complex display lower fluctuations than those in the context of the Grb2–PR–Grb2 complex (Fig. 6C). These differences are particularly pronounced for residues within and flanking the G1 and G2 motifs located within the PR domain. Thus, whereas residues within and flanking the G1 and G2 motifs in the context of the $(Grb2)_2$–PR complex fluctuate with an rmsf of < 3 Å, the corresponding residues in the context of the Grb2–PR–Grb2 complex do so with a rmsf of > 5 Å. Taking the findings together, our MD analysis supports the notion

that Grb2 most likely binds to the PR domain of Gab1 as a homodimer, so as to form the $(Grb2)_2$–PR complex in lieu of two independent monomers.

Conclusions

Multivalent binding is a hallmark of biological systems and, in particular, is a common feature of proteins involved in mediating cellular signaling cascades. It is generally believed that multivalency provides a physical mechanism to drive the binding of cellular partners in a synergistic and cooperative manner. Such allosteric behavior allows proteins to fine-tune their activity in response to rapidly fluctuating cellular conditions and external stimuli. Thus, for example, binding at one site not only increases the local concentration of two interacting partners, but may also lower the entropic penalty for binding at a second site in a cooperative manner. The resulting enhancement in binding affinity provides the basis for positive cooperativity. On the other hand, binding at one site may either induce conformational changes within a protein, such that binding at a second site is compromised, or sterically hinder binding at a second site, through negative cooperativity. Finally, multivalent binding may also be driven in a manner such that binding at multiple sites occurs independently in the absence of any cooperativity. Our present study shows that the bivalent binding of the Grb2 adaptor to two distinct RXXK sites within the Gab1 docking protein is governed by this so-called zero cooperativity.

We note that the lack of cooperativity observed in driving the assembly of the Grb2–Gab1 macromolecular complex does not necessarily imply a lack of allosteric communication. On the contrary, our previous work has shown that the formation of the Sos1–Grb2–Gab1 ternary complex is under tight allosteric control [41]. Specifically, our previous findings revealed that the binding of one molecule of Sos1 to the nSH3 domain allosterically induces a conformational change within Grb2, such that the loading of a second molecule of Sos1 onto the cSH3 domain is blocked, allowing Gab1 to have access to the cSH3 domain in an exclusively noncompetitive manner to generate the Sos1–Grb2–Gab1 ternary signaling complex. Indeed, it is unlikely that the Grb2–Gab1 complex exists in isolation in the context of the cellular milieu, and, under any given conditions, Gab1 most likely binds to Grb2 in association with other cellular components such as Sos1.

Importantly, our reductionist approach to understanding the assembly of the Grb2–Gab1 complex in isolation from other interacting partners has provided novel insights that would have been difficult to obtain from studies on live cells, and the complexity of the cellular milieu would have blurred the clear picture presented here. Indeed, despite its key role in driving a multitude of cellular signaling cascades [1–3], the mechanism underpinning the assembly of the Grb2–Gab1 complex has hitherto remained poorly understood. In an effort to lay the groundwork for remedying this situation, we have demonstrated here that the Grb2–Gab1 interaction is mediated by the binding of the cSH3 domain within two individual Grb2 molecules to two distinct RXXK motifs, designated G1 and G2, within the PR domain of Gab1. Although the binding of Grb2 to Gab1 as two independent monomers (Grb2–PR–Grb2) is physically possible, our MD simulations support a model whereby the formation of this complex would preferentially occur via the binding of the Grb2 homodimer to Gab1 to generate the $(Grb2)_2$–PR ternary complex. Given the fact that Grb2 exists in a monomer–dimer equilibrium in solution, it is equally plausible that binding of Gab1 to the Grb2 homodimer simply shifts this equilibrium in its favor. Nonetheless, the possibility that Grb2 monomers associate into a homodimer upon binding to Gab1 cannot be excluded. Importantly, the monomers within the Grb2 homodimer adopt a two-fold axis of symmetry, such that the SH2 domain of one monomer docks against the cSH3 domain of the other and vice versa in a head-to-tail fashion, as observed in the crystal structure determined by Ducruix *et al.* [31]. Our previous studies have shown that Grb2 monomers most likely undergo structural rearrangement, with respect to the spatial orientation of various domains within the nSH3–SH2–cSH3 modular cassette, so as to adopt a conformation that is somewhat topologically distinct from and thermodynamically more stable than that observed in the context of the Grb2 homodimer [30]. Although no experimental data are available, we speculate that the integrity of both the SH2 and cSH3 domains is critical for the dimerization of Grb2.

We add that our present study fails to adequately address whether binding of Grb2 to two RXXK motifs within Gab1 occurs in an ordered or random manner. Although the data presented herein unequivocally demonstrate that Gab1 contains a high-affinity G2 site and a low-affinity G1 site for latching onto Grb2, it is unlikely that binding of these sites to Grb2 occurs in an ordered manner, in light of the fact that both of these sites appear to bind to Grb2 in an independent manner with zero cooperativity. It is noteworthy that the G1 and G2 motifs flank the binding site for the MET and RON RTKs within the PR domain of Gab1 [17,42,43]. Given that Gab1 can be recruited to the inner membrane surface via binding to Grb2 or through its direct interaction with the cytoplasmic tails of MET and

RON receptors, we believe that Gab1–MET/RON and Gab1–Grb2 interactions are likely to be mutually exclusive. Thus, binding of Grb2 to Gab1 would most likely prevent subsequent binding of MET/RON via steric hindrance and vice versa. Accordingly, the cellular ratio of Grb2 probably determines whether coupling of Gab1 to MET/RON occurs directly or via the Grb2–Gab1 interaction, with important consequences for the downstream signaling pathways involved in a diverse array of cellular activities [42,44]. In addition to competition between the Grb2 adaptor and MET/RON receptors for binding to Gab1, post-translational modifications may provide additional regulatory layers for mediating this competition and/or providing access to a plethora of other cellular partners of Gab1. Thus, for example, recent work by Eulenfeld and Schaper showed that MAPK-dependent phosphorylation of Ser551 located within the C-terminus of Gab1 is required for its recruitment to the inner membrane surface via its PH domain [45]. It is thus conceivable that the C-terminus, including the PR domain, somehow associates with the N-terminal PH domain in an intramolecular autoinhibitory fashion under quiescent cellular conditions, and that such inhibition is only relieved upon the activation of the MAPK cascade. Likewise, access of other cellular partners to the PR domain of Gab1 may also be blocked until after receptor stimulation. Collectively, these observations epitomize the role of interacting partners and regulatory switches in dictating the accessibility of Grb2 to G1 and G2 motifs within the PR domain of Gab1.

Together with Gab1, Gab2 and Gab3 constitute the Gab family of proteins, which are implicated in coupling activated RTKs to downstream signaling cascades involved in a myriad of cellular activities [1–3]. Importantly, the role of Gab proteins in RTK signaling does not appear to be redundant nor are they dispensable. Could functional differences between Gab proteins be accounted for in terms of their structural organization? Interestingly, whereas all three members of the Gab family contain highly conserved G1 and G2 motifs for the recruitment of Grb2, the binding site for MET/RON receptors is unique to Gab1, being absent from Gab2 and Gab3. Consistent with this observation, disruption of the *Gab1* gene in mice results in developmental defects in a manner akin to *MET* gene knockout [7,8,46], implying that Gab1 has a nonredundant role in coupling signaling from the MET receptor. Feller *et al.* recently characterized the structural basis for the binding of the cSH3 domain of Grb2 to the G1 and G2 motifs derived from Gab2 [47]. Their work indicated that, whereas the G1 motif adopts a PPII helical conformation upon binding to the cSH3 domain, the G2 motif adopts a 3_{10}-helical conformation. Given that the G1 and G2 motifs are almost completely conserved in both Gab1 and Gab2, we have proposed herein a similar mechanism for the interaction of Grb2 with Gab1, in line with this previous study. Thus, although Gab1 may be nonredundant for signaling through the MET receptor, we believe that it may be dispensable for signaling through Grb2. However, we note that other functional differences between Gab proteins may also arise from their ability to be targeted for post-translational modifications by upstream effectors such as the MAPK cascade.

Finally, we note that, owing to difficulties associated with the purification of full-length Gab1, the insights into the assembly of the Grb2–Gab1 signaling complex presented here are largely drawn from the isolated PR domain. Although the possibility that the PR domain might behave in a different manner in the context of intact Gab1, in terms of both its conformation and its ligand binding, we believe that our new findings lay the groundwork for future studies despite such shortcomings. In sum, our study sheds new light on the physicochemical forces driving the assembly of a key macromolecular signaling complex that is relevant to cellular health and disease.

Experimental procedures

Sample preparation

Full-length human Grb2 (residues 1–217; UniProt no. P62993) and the PR domain of human Gab1 (residues 331–530; UniProt no. Q13480) were cloned into pET30 bacterial expression vectors with an N-terminal His-tag, by use of Novagen LIC technology (Novagen, Madison, WI, USA). Additionally, various mutant constructs of full-length Grb2 and the PR domain of Gab1 were generated through *de novo* cDNA synthesis, courtesy of the GenScript Corporation (GenScript, Piscataway, NJ, USA), or alternatively with the PCR primer extension method [48] (Fig. 1). All recombinant constructs were expressed in *Escherichia coli* BL21*(DE3) (Invitrogen, Carlsbad, CA, USA), and purified on an Ni^{2+}–nitrilotriacetic acid affinity column, with standard procedures. Briefly, bacterial cells were grown at 20 °C in Terrific Broth to an attenuance of greater than unity at 600 nm, prior to induction with 0.5 mM isopropyl thio-β-D-galactoside. The bacterial culture was further grown overnight at 20 °C, and the cells were subsequently harvested and disrupted with a BeadBeater (Biospec, Bartlesville, OK, USA). After separation of cell debris by high-speed centrifugation (30 000 ***g*** for 30 min), the cell lysate was loaded onto an Ni^{2+}–nitrilotriacetic acid column and washed extensively with 20 mM imidazole to remove nonspecific bacterial proteins bound to the column.

The recombinant proteins were subsequently eluted with 200 mM imidazole and dialyzed against an appropriate buffer to remove excess imidazole. Further treatment on a Hiload Superdex 200 size-exclusion chromatography column coupled in-line with a GE Akta FPLC system (GE Healthcare, Milwaukee, WI, USA) led to the purification of various constructs of Grb2 and the PR domain of Gab1 to apparent homogeneity, as judged by SDS/PAGE analysis. Final yields were typically between 10 and 20 mg of protein of apparent homogeneity per liter of bacterial culture. Treatment with thrombin protease to remove the N-terminal His-tag destabilized the recombinant proteins, and they appeared to be proteolytically unstable. For this reason, except for control experiments to ensure that the His-tag had no effect on protein conformation and ligand binding, all experiments reported herein were carried out on fusion constructs with an N-terminal His-tag. The protein concentration was determined with the fluorescence-based Quant-It assay (Invitrogen), and spectrophotometrically on the basis of extinction coefficients calculated for each recombinant construct with the online software PROTPARAM at the ExPasy server [49]. Results from both methods were in an excellent agreement.

ALS

ALS experiments were conducted on a Wyatt miniDAWN TREOS triple-angle static light scattering (SLS) detector (Wyatt Technology, Santa Barbara, CA, USA) and a Wyatt QELS dynamic light scattering (DLS) detector coupled in-line with a Wyatt Optilab rEX differential refractive index detector and interfaced to a Hiload Superdex 200 size-exclusion chromatography column under the control of a GE Akta FPLC system within a chromatography refrigerator at 10 °C. Protein samples of various constructs of > full-length Grb2 and the PR domain of Gab1 were prepared in 50 mM Tris, 200 mM NaCl, 1 mM EDTA and 5 mM β-mercaptoethanol at pH 8.0, and loaded onto the column at a flow rate of 1 mL·min^{-1}; the data were automatically acquired with ASTRA. The starting concentrations injected onto the column were typically between 40 and 50 μM for each protein construct. The angular and concentration dependence of the SLS intensity of each protein species resolved in the flow mode was measured with the Wyatt miniDAWN TREOS detector. The SLS data were analyzed according to the following built-in Zimm equation in ASTRA [50,51]:

$$(Kc/R_\theta) = [(1/M) + 2A_2c](1 + \{[16\pi^2(R_g)^2/3\lambda^2]\sin^2(\theta/2)\}) \quad (1)$$

where R_θ is the excess Raleigh ratio attributable to protein in the solution as a function of protein concentration c (mg·mL^{-1}) and the scattering angle θ (42°, 90°, and 138°), M is the observed molar mass of each protein species, A_2 is the second virial coefficient, λ is the wavelength of laser light in solution (658 nm), R_g is the radius of gyration of the protein, and K is given by the following relationship:

$$K = [4\pi^2 n^2 (dn/dc)^2]/N_A\lambda^4 \quad (2)$$

where n is the refractive index of the solvent, dn/dc is the refractive index increment of the protein in solution, and N_A is Avogadro's number (6.02×10^{23} mol^{-1}). With low protein concentrations ($c \rightarrow 0$), Eqn (1) reduces to:

$$(Kc/R_\theta) = (1/M) + \{[16\pi^2(R_g)^2/3M\lambda^2]\sin^2(\theta/2)\} \quad (3)$$

Thus, a plot of (Kc/R_θ) versus $\sin^2(\theta/2)$ yields a straight line with slope $16\pi^2R_g^2/3M\lambda^2$ and y-intercept $1/M$. Accordingly, molar mass can be obtained in a global analysis from the y-intercept of linear fits of a range of (Kc/R_θ) – $\sin^2(\theta/2)$ plots as a function of protein concentration along the elution profile of each protein species, by use of SLS measurements at three scattering angles. Weighted-average molar mass (M_w) and number-average molar mass (M_n) were calculated from the following relationships:

$$M_w = \Sigma(c_iM_i)/\Sigma c_i \quad (4)$$

$$M_n = \Sigma c_i/\Sigma(c_i/M_i) \quad (5)$$

where c_i is the protein concentration and M_i is the observed molar mass at the ith slice within an elution profile. It should, however, be noted that R_g could not be determined for any protein species, owing to the lack of angular dependence of scattered light. The time and concentration dependence of DLS intensity fluctuation of each protein species resolved in the flow mode was measured with the Wyatt QELS detector positioned at 90° with respect to the incident laser beam. The DLS data were iteratively fitted by the use of nonlinear least squares regression analysis to the following built-in equation in ASTRA [52–54]:

$$G(\tau) = \alpha\mathrm{Exp}(-2\Gamma\tau) + \beta \quad (6)$$

where $G(\tau)$ is the autocorrelation function of DLS intensity fluctuation I, τ is the delay time of the autocorrelation function, Γ is the decay rate constant of the autocorrelation function, α is the initial amplitude of the autocorrelation function at zero delay time, and β is the baseline offset (the value of the autocorrelation function at infinite delay time). Thus, fitting the above equation to a range of $G(\tau)$ – τ plots as a function of protein concentration along the elution profile of each protein species computes the weighted-average value of Γ using DLS measurements at a scattering angle of 90°. Accordingly, the translational diffusion coefficient (D_t) of each protein species was calculated from the following relationship:

$$D_t = (\Gamma\lambda^2)/[16\pi^2n^2\sin^2(\theta/2)] \quad (7)$$

where λ is the wavelength of laser light in solution (658 nm), n is the refractive index of the solvent, and θ is the scattering

angle (90°). Additionally, the hydrodynamic radius (R_h) of each protein construct can be determined from the Stokes–Einstein relationship:

$$R_h = (k_B T)/(6\pi\eta D_t) \quad (8)$$

where k_B is Boltzman's constant (1.38×10^{-23} J·K^{-1}), T is the absolute temperature, and η is the solvent viscosity. We note that the R_h reported here represents the weighted-average value as defined by the following expression:

$$R_h = \Sigma(c_i R_{h,i})/\Sigma c_i \quad (9)$$

where c_i is the protein concentration and $R_{h,i}$ is the observed hydrodynamic radius at the ith slice within an elution profile. It should also be noted that, in both the SLS and DLS measurements, the protein concentration (c) along the elution profile of each protein species was automatically quantified in ASTRA from the change in refractive index (Δn) with respect to the solvent as measured by the Wyatt Optilab rEX detector with the following relationship:

$$c = (\Delta n)/(dn/dc) \quad (10)$$

where dn/dc is the refractive index increment of the protein in solution.

ITC

ITC measurements were performed on a Microcal VP-ITC instrument (MicroCal, Northampton, MA, USA), and data were acquired and processed with the fully automized features in Microcal ORIGIN. Briefly, protein samples were prepared in 50 mM Tris, 200 mM NaCl, 1 mM EDTA and 5 mM β-mercaptoethanol at pH 8.0. The experiments were initiated by injecting 25 10-μL aliquots of 0.5–1 mM of each construct of the PR domain of Gab1 from the syringe into the calorimetric cell containing 1.8 mL of 50–100 μM full-length Grb2 solution at 25 °C. The change in thermal power as a function of each injection was automatically recorded with ORIGIN, and the raw data were further processed to yield binding isotherms of heat release per injection as a function of the molar ratio of each PR construct to full-length Grb2. The heats of mixing and dilution were subtracted from the heat of binding per injection by carrying out a control experiment in which the same buffer in the calorimetric cell was titrated against each PR construct in an identical manner. To extract binding affinity (K_d) and binding enthalpy (ΔH), the ITC isotherms were iteratively fitted by the use of nonlinear least squares regression analysis with the following built-in equation in ORIGIN:

$$q(i) = (\Delta HVP/2n)([1 + (nL/P) + (nK_d/P)] - \{[1 + (nL/P) + (nK_d/P)]^2 - (4nL/P)\}^{1/2}) \quad (11)$$

where $q(i)$ is the heat release (kcal·mol^{-1}) for the ith injection, V is the effective volume of protein solution in the calorimetric cell (1.46 mL), P is the total concentration of full-length Grb2 in the calorimetric cell, L is the total concentration of each PR construct added from the syringe for the ith injection, and n is the stoichiometry of full-length Grb2 bound to each PR construct at equilibrium. The above equation is derived from the binding of a ligand to a macromolecule by using the law of mass action, assuming a one-site model [55]. The free energy change (ΔG) upon the binding of Grb2 to each PR construct was calculated from the relationship:

$$\Delta G = nRT \ln K_d \quad (12)$$

where n is the integral number of binding sites within the PR domain or the observed stoichiometry of binding of Grb2 to the PR domain, R is the universal molar gas constant (1.99 cal·K^{-1}·mol^{-1}), and T is the absolute temperature. The entropic contribution ($T\Delta S$) to the free energy of binding was calculated from the relationship:

$$T\Delta S = \Delta H - \Delta G \quad (13)$$

where ΔH and ΔG are as defined above. The free energy of cooperativity ($\Delta\Delta G_c$), resulting from the bivalent binding of Grb2 to the G1 and G2 sites within the PR domain of Gab1, was calculated from the following relationship:

$$\Delta\Delta G_c = (\Delta G_{wt}) - (\Delta G_{m2} + \Delta G_{m1}) \quad (14)$$

where ΔG_{m2} is the free energy change associated with the binding of Grb2 to the G1 site within the PR_mG2 construct (G2 site mutated), ΔG_{m1} is the free energy change associated with the binding of Grb2 to the G2 site within the PR_mG1 construct (G1 site mutated), and ΔG_{wt} is the free energy change associated with the binding of Grb2 to both the G1 and G2 site within PR_WT.

CD

Far-UV CD measurements were conducted on a Jasco J-815 spectrometer (Jasco, Easton, MD, USA) thermostatically controlled at 25 °C. Experiments were conducted on 5 μM of the wild-type PR domain of Gab1 in 10 mM sodium phosphate containing 5 mM β-mercaptoethanol at pH 8.0. Notably, despite its undesirable absorption in the far-UV region, the inclusion of β-mercaptoethanol in the buffer was necessary to prevent interchain crosslinking of the PR domain of Gab1 resulting from rapid oxidation of thiol moieties of several cysteines. Data were collected by use of a quartz cuvette with a 2-mm pathlength in the 190–250-nm wavelength range. Data were normalized against reference spectra to remove the contribution of buffer. Data were recorded with a slit bandwidth of 2 nm at a scan rate of 10 nm·min^{-1}. Each dataset represents an average of four scans acquired at 0.1-nm intervals. Data were converted to molar ellipticity, [θ], as a function of the wavelength (λ) of electromagnetic radiation, with the equation:

$$[\theta] = [(10^5 \Delta\varepsilon)/cl] \text{ deg cm}^2 \cdot \text{dmol}^{-1} \quad (15)$$

where $\Delta\varepsilon$ is the observed ellipticity (mdeg), c is the protein concentration (μM), and l is the cuvette pathlength (cm).

Molecular modeling

Molecular modeling was employed to construct structural models of Grb2 in complex with the PR domain of Gab1 either as two independent monomers (Grb2–PR–Grb2), or in the context of a homodimer [$(Grb2)_2$–PR], on the basis of homology modeling, with MODELLER [56]. Briefly, the atomic models were built in various stages. First, the intervening polypeptide chain spanning the G1 and G2 sites within the PR domain of Gab1 was folded into a compact globular-like topology with the QUARK server, on the basis of *ab initio* modeling. The QUARK server can be accessed online at http://zhanglab.ccmb.med.umich.edu/quark. Notably, *ab initio* modeling was motivated by the fact that the PR domain of Gab1 appears to be structurally compact on the basis of our hydrodynamic data presented here. Next, the $(Grb2)_2$–PR structural model was built by using the *ab initio* structural model of the PR domain in combination with the crystal structure of the Grb2 homodimer alone [Protein Data Bank (PDB) 1GRI], the crystal structure of the isolated cSH3 domain of Grb2 bound to an RXXK motif homologous to the G1 site (PDB 2W0Z), and the crystal structure of the isolated cSH3 domain of Grb2 bound to an RXXK motif homologous to the G2 site (PDB 2VWF), by use of the multiple-template alignment strategy in MODELLER [56]. Additionally, hydrogen bonding restraints between consensus arginine and lysine (Arg344/Lys347) within the G1 site and Glu171/Glu174 within the cSH3 domain of one monomer of Grb2, as well as between consensus arginine and lysine (Arg521/Lys524) within the G2 site and Glu171/Glu174 within the nSH3 domain of second monomer of Grb2, were introduced as described previously [29]. The Grb2–PR–Grb2 structural model was derived from the prebuilt structural model of $(Grb2)_2$–PR. Here, the intervening polypeptide chain spanning the G1 and G2 sites within the PR domain of Gab1 was excised out, and the two monomers within the Grb2 homodimer bound to isolated G1 and G2 sites were spatially displaced and moved apart laterally in a rigid-body fashion, so as to deplete them of any intermonomer contacts in MOLMOL [57]. The resulting conformation of two noninteracting Grb2 monomers in complex with isolated G1 and G2 sites in combination with the *ab initio* structural model of the PR domain were subsequently used as templates to construct the Grb2–PR–Grb2 structural model in MODELLER [56]. In each case, a total of 100 structural models were calculated, and the structure with the lowest energy, as judged by the MODELLER Objective Function, was selected for further analysis. The modeled structures were rendered with RIBBONS [58]. All calculations and data processing were performed on a Linux workstation equipped with a dual-core processor.

MD

MD simulations were performed with GROMACS [59,60], using the integrated OPLS-AA force field [61,62]. Briefly, the modeled structures of Grb2 in complex with the PR domain of Gab1 as two independent monomers (Grb2–PR–Grb2) and in the context of a homodimer [$(Grb2)_2$–PR] were centered within a cubic box, and hydrated with the extended simple point charge water model [63,64]. The hydrated structures were energy-minimized with the steepest descent algorithm prior to equilibration under the NPT ensemble conditions, wherein the number of atoms (N), pressure (P) and temperature (T) within the system were, respectively, kept constant at $\sim 10^5$, 1 bar, and 300 K. The particle-mesh Ewald method was employed to compute long-range electrostatic interactions with a 10-Å cut-off [65], and the Linear Constraint Solver (LINCS) algorithm was employed to restrain bond lengths [66]. All MD simulations were performed under periodic boundary conditions, with the leap-frog integrator with a time step of 2 fs. For the final MD production runs, data were collected every 10 ps over a time scale of 50 ns. All simulations were run on a Linux workstation with parallel processors at the High Performance Computing facility within the Center for Computational Science of the University of Miami.

Acknowledgements

This work was supported by funds from the National Institutes of Health (Grant R01-GM083897) and the USylvester Braman Family Breast Cancer Institute to A. Farooq. C. B. McDonald is a recipient of a postdoctoral fellowship from the National Institutes of Health (Award T32-CA119929).

References

1 Gu H & Neel BG (2003) The 'Gab' in signal transduction. *Trends Cell Biol* **13**, 122–130.
2 Liu Y & Rohrschneider LR (2002) The gift of Gab. *FEBS Lett* **515**, 1–7.
3 Nishida K & Hirano T (2003) The role of Gab family scaffolding adapter proteins in the signal transduction of cytokine and growth factor receptors. *Cancer Sci* **94**, 1029–1033.
4 Wohrle FU, Daly RJ & Brummer T (2009) How to Grb2 a Gab. *Structure* **17**, 779–781.
5 Vaughan TY, Verma S & Bunting KD (2011) Grb2-associated binding (Gab) proteins in hematopoietic and immune cell biology. *Am J Blood Res* **1**, 130–134.

6 Simister PC & Feller SM (2012) Order and disorder in large multi-site docking proteins of the Gab family – implications for signalling complex formation and inhibitor design strategies. *Mol BioSyst* **8**, 33–46.
7 Itoh M, Yoshida Y, Nishida K, Narimatsu M, Hibi M & Hirano T (2000) Role of Gab1 in heart, placenta, and skin development and growth factor- and cytokine-induced extracellular signal-regulated kinase mitogen-activated protein kinase activation. *Mol Cell Biol* **20**, 3695–3704.
8 Sachs M, Brohmann H, Zechner D, Muller T, Hulsken J, Walther I, Schaeper U, Birchmeier C & Birchmeier W (2000) Essential role of Gab1 for signaling by the c-Met receptor in vivo. *J Cell Biol* **150**, 1375–1384.
9 Cheng AM, Saxton TM, Sakai R, Kulkarni S, Mbamalu G, Vogel W, Tortorice CG, Cardiff RD, Cross JC, Muller WJ *et al.* (1998) Mammalian Grb2 regulates multiple steps in embryonic development and malignant transformation. *Cell* **95**, 793–803.
10 Meng S, Chen Z, Munoz-Antonia T & Wu J (2005) Participation of both Gab1 and Gab2 in the activation of the ERK/MAPK pathway by epidermal growth factor. *Biochem J* **391**, 143–151.
11 Daly RJ, Binder MD & Sutherland RL (1994) Overexpression of the Grb2 gene in human breast cancer cell lines. *Oncogene* **9**, 2723–2727.
12 Tari AM, Hung MC, Li K & Lopez-Berestein G (1999) Growth inhibition of breast cancer cells by Grb2 down-regulation is correlated with inactivation of mitogen-activated protein kinase in EGFR, but not in ErbB2, cells. *Oncogene* **18**, 1325–1332.
13 Rozakis-Adcock M, McGlade J, Mbamalu G, Pelicci G, Daly R, Li W, Batzer A, Thomas S, Brugge J, Pelicci PG *et al.* (1992) Association of the Shc and Grb2/Sem5 SH2-containing proteins is implicated in activation of the Ras pathway by tyrosine kinases. *Nature* **360**, 689–692.
14 Lowenstein EJ, Daly RJ, Batzer AG, Li W, Margolis B, Lammers R, Ullrich A, Skolnik EY, Bar-Sagi D & Schlessinger J (1992) The SH2 and SH3 domain-containing protein GRB2 links receptor tyrosine kinases to ras signaling. *Cell* **70**, 431–442.
15 Chardin P, Camonis JH, Gale NW, van Aelst L, Schlessinger J, Wigler MH & Bar-Sagi D (1993) Human Sos1: a guanine nucleotide exchange factor for Ras that binds to GRB2. *Science* **260**, 1338–1343.
16 Li N, Batzer A, Daly R, Yajnik V, Skolnik E, Chardin P, Bar-Sagi D, Margolis B & Schlessinger J (1993) Guanine-nucleotide-releasing factor hSos1 binds to Grb2 and links receptor tyrosine kinases to Ras signalling. *Nature* **363**, 85–88.
17 Schaeper U, Gehring NH, Fuchs KP, Sachs M, Kempkes B & Birchmeier W (2000) Coupling of Gab1 to c-Met, Grb2, and Shp2 mediates biological responses. *J Cell Biol* **149**, 1419–1432.
18 Lewitzky M, Kardinal C, Gehring NH, Schmidt EK, Konkol B, Eulitz M, Birchmeier W, Schaeper U & Feller SM (2001) The C-terminal SH3 domain of the adapter protein Grb2 binds with high affinity to sequences in Gab1 and SLP-76 which lack the SH3-typical P-x-x-P core motif. *Oncogene* **20**, 1052–1062.
19 Seedorf K, Kostka G, Lammers R, Bashkin P, Daly R, Burgess WH, van der Bliek AM, Schlessinger J & Ullrich A (1994) Dynamin binds to SH3 domains of phospholipase C gamma and GRB-2. *J Biol Chem* **269**, 16009–16014.
20 Vidal M, Montiel JL, Cussac D, Cornille F, Duchesne M, Parker F, Tocque B, Roques BP & Garbay C (1998) Differential interactions of the growth factor receptor-bound protein 2 N-SH3 domain with son of sevenless and dynamin. Potential role in the Ras-dependent signaling pathway. *J Biol Chem* **273**, 5343–5348.
21 Odai H, Sasaki K, Iwamatsu A, Hanazono Y, Tanaka T, Mitani K, Yazaki Y & Hirai H (1995) The proto-oncogene product c-Cbl becomes tyrosine phosphorylated by stimulation with GM-CSF or Epo and constitutively binds to the SH3 domain of Grb2/Ash in human hematopoietic cells. *J Biol Chem* **270**, 10800–10805.
22 Park RK, Kyono WT, Liu Y & Durden DL (1998) CBL–GRB2 interaction in myeloid immunoreceptor tyrosine activation motif signaling. *J Immunol* **160**, 5018–5027.
23 Moeller SJ, Head ED & Sheaff RJ (2003) p27Kip1 inhibition of GRB2-SOS formation can regulate Ras activation. *Mol Cell Biol* **23**, 3735–3752.
24 Robinson MJ & Cobb MH (1997) Mitogen-activated protein kinase pathways. *Curr Opin Cell Biol* **9**, 180–186.
25 Cunnick JM, Meng S, Ren Y, Desponts C, Wang HG, Djeu JY & Wu J (2002) Regulation of the mitogen-activated protein kinase signaling pathway by SHP2. *J Biol Chem* **277**, 9498–9504.
26 Araki T, Nawa H & Neel BG (2003) Tyrosyl phosphorylation of Shp2 is required for normal ERK activation in response to some, but not all, growth factors. *J Biol Chem* **278**, 41677–41684.
27 Kim D & Chung J (2002) Akt: versatile mediator of cell survival and beyond. *J Biochem Mol Biol* **35**, 106–115.
28 Lock LS, Royal I, Naujokas MA & Park M (2000) Identification of an atypical Grb2 carboxyl-terminal SH3 domain binding site in Gab docking proteins reveals Grb2-dependent and -independent recruitment of Gab1 to receptor tyrosine kinases. *J Biol Chem* **275**, 31536–31545.
29 McDonald CB, Seldeen KL, Deegan BJ, Bhat V & Farooq A (2011) Binding of the cSH3 domain of Grb2 adaptor to two distinct RXXK motifs within Gab1 docker employs differential mechanisms. *J Mol Recognit* **24**, 585–596.

30 McDonald CB, Seldeen KL, Deegan BJ, Lewis MS & Farooq A (2008) Grb2 adaptor undergoes conformational change upon dimerization. *Arch Biochem Biophys* **475**, 25–35.
31 Maignan S, Guilloteau JP, Fromage N, Arnoux B, Becquart J & Ducruix A (1995) Crystal structure of the mammalian Grb2 adaptor. *Science* **268**, 291–293.
32 Dunker AK, Lawson JD, Brown CJ, Williams RM, Romero P, Oh JS, Oldfield CJ, Campen AM, Ratliff CM & Hipps KW (2001) Intrinsically disordered protein. *J Mol Graph Model* **19**, 26–59.
33 Dunker AK, Cortese MS, Romero P, Iakoucheva LM & Uversky VN (2005) Flexible nets. The roles of intrinsic disorder in protein interaction networks. *FEBS J* **272**, 5129–5148.
34 Liu J, Perumal NB, Oldfield CJ, Su EW, Uversky VN & Dunker AK (2006) Intrinsic disorder in transcription factors. *Biochemistry* **45**, 6873–6888.
35 Haynes C, Oldfield CJ, Ji F, Klitgord N, Cusick ME, Radivojac P, Uversky VN, Vidal M & Iakoucheva LM (2006) Intrinsic disorder is a common feature of hub proteins from four eukaryotic interactomes. *PLoS Comput Biol* **2**, e100.
36 Uversky VN (2011) Intrinsically disordered proteins from A to Z. *Int J Biochem Cell Biol* **43**, 1090–1103.
37 Shimizu K, Hirose S & Noguchi T (2007) POODLE-S: web application for predicting protein disorder by using physicochemical features and reduced amino acid set of a position-specific scoring matrix. *Bioinformatics* **23**, 2337–2338.
38 Rabanal F, Ludevid MD, Pons M & Giralt E (1993) CD of proline-rich polypeptides: application to the study of the repetitive domain of maize glutelin-2. *Biopolymers* **33**, 1019–1028.
39 Kelly SM, Jess TJ & Price NC (2005) How to study proteins by circular dichroism. *Biochim Biophys Acta* **1751**, 119–139.
40 Renzoni DA, Pugh DJ, Siligardi G, Das P, Morton CJ, Rossi C, Waterfield MD, Campbell ID & Ladbury JE (1996) Structural and thermodynamic characterization of the interaction of the SH3 domain from Fyn with the proline-rich binding site on the p85 subunit of PI3-kinase. *Biochemistry* **35**, 15646–15653.
41 McDonald CB, Seldeen KL, Deegan BJ, Bhat V & Farooq A (2010) Assembly of the Sos1–Grb2–Gab1 ternary signaling complex is under allosteric control. *Arch Biochem Biophys* **494**, 216–225.
42 Schaeper U, Vogel R, Chmielowiec J, Huelsken J, Rosario M & Birchmeier W (2007) Distinct requirements for Gab1 in Met and EGF receptor signaling in vivo. *Proc Natl Acad Sci USA* **104**, 15376–15381.
43 Chaudhuri A, Xie MH, Yang B, Mahapatra K, Liu J, Marsters S, Bodepudi S & Ashkenazi A (2011) Distinct involvement of the Gab1 and Grb2 adaptor proteins in signal transduction by the related receptor tyrosine kinases RON and MET. *J Biol Chem* **286**, 32762–32774.
44 Wagh PK, Peace BE & Waltz SE (2008) Met-related receptor tyrosine kinase Ron in tumor growth and metastasis. *Adv Cancer Res* **100**, 1–33.
45 Eulenfeld R & Schaper F (2009) A new mechanism for the regulation of Gab1 recruitment to the plasma membrane. *J Cell Sci* **122**, 55–64.
46 Rosario M & Birchmeier W (2003) How to make tubes: signaling by the Met receptor tyrosine kinase. *Trends Cell Biol* **13**, 328–335.
47 Harkiolaki M, Tsirka T, Lewitzky M, Simister PC, Joshi D, Bird LE, Jones EY, O'Reilly N & Feller SM (2009) Distinct binding modes of two epitopes in Gab2 that interact with the SH3C domain of Grb2. *Structure* **17**, 809–822.
48 Gao X, Yo P, Keith A, Ragan TJ & Harris TK (2003) Thermodynamically balanced inside-out (TBIO) PCR-based gene synthesis: a novel method of primer design for high-fidelity assembly of longer gene sequences. *Nucleic Acids Res* **31**, e143.
49 Gasteiger E, Hoogland C, Gattiker A, Duvaud S, Wilkins MR, Appel RD & Bairoch A (2005) Protein identification and analysis tools on the ExPASy Server. In *The Proteomics Protocols Handbook* (Walker JM ed.), pp. 571–607. Humana Press, Totowa, NJ.
50 Zimm BH (1948) The scattering of light and the radial distribution function of high polymer solutions. *J Chem Phys* **16**, 1093–1099.
51 Wyatt PJ (1993) Light scattering and the absolute characterization of macromolecules. *Anal Chim Acta* **272**, 1–40.
52 Berne BJ & Pecora R (1976) *Dynamic Light Scattering*. Wiley, New York.
53 Chu B (1991) *Laser Light Scattering: Basic Principles and Practice*. Academic, Boston.
54 Koppel DE (1972) Analysis of macromolecular polydispersity in intensity correlation spectroscopy. *J Chem Phys* **57**, 4814–4820.
55 Wiseman T, Williston S, Brandts JF & Lin LN (1989) Rapid measurement of binding constants and heats of binding using a new titration calorimeter. *Anal Biochem* **179**, 131–137.
56 Marti-Renom MA, Stuart AC, Fiser A, Sanchez R, Melo F & Sali A (2000) Comparative protein structure modeling of genes and genomes. *Annu Rev Biophys Biomol Struct* **29**, 291–325.
57 Koradi R, Billeter M & Wuthrich K (1996) MOLMOL: a program for display and analysis of macromolecular structures. *J Mol Graph* **14**, 51–55.
58 Carson M (1991) Ribbons 2.0. *J Appl Crystallogr* **24**, 958–961.
59 Van Der Spoel D, Lindahl E, Hess B, Groenhof G, Mark AE & Berendsen HJ (2005) GROMACS: fast, flexible, and free. *J Comput Chem* **26**, 1701–1718.

60 Hess B (2008) GROMACS 4: algorithms for highly efficient, load-balanced, and scalable molecular simulation. *J Chem Theory Comput* **4**, 435–447.
61 Jorgensen WL & Tirado-Rives J (1988) The OPLS force field for proteins: energy minimizations for crystals of cyclic peptides and crambin. *J Am Chem Soc* **110**, 1657–1666.
62 Kaminski GA, Friesner RA, Tirado-Rives J & Jorgensen WL (2001) Evaluation and reparametrization of the OPLS-AA force field for proteins via comparison with accurate quantum chemical calculations on peptides. *J Phys Chem B* **105**, 6474–6487.
63 Toukan K & Rahman A (1985) Molecular-dynamics study of atomic motions in water. *Phys Rev B* **31**, 2643–2648.
64 Berendsen HJC, Grigera JR & Straatsma TP (1987) The missing term in effective pair potentials. *J Phys Chem* **91**, 6269–6271.
65 Darden TA, York D & Pedersen L (1993) Particle mesh Ewald: an N.log(N) method for Ewald sums in large systems. *J Chem Phys* **98**, 10089–10092.
66 Hess B, Bekker H, Berendsen HJC & Fraaije JGEM (1997) LINCS: a linear constraint solver for molecular simulations. *J Comput Chem* **18**, 1463–1472.